

Direct solutions of the Si(111) 7×7 structure

C.J. Gilmore ^{a,*}, L.D. Marks ^b, D. Grozea ^b, C. Collazo ^b, E. Landree ^b, R.D. Twesten ^{c,1}

^a Department of Chemistry, University of Glasgow, Glasgow G12 8QQ, UK

^b Department of Materials Science and Engineering, Northwestern University, Evanston, IL 60208, USA

^c Department of Physics, University of Illinois, Urbana, IL 61801, USA

Received 6 September 1996; accepted for publication 26 December 1996

Abstract

We show that it is possible to use direct methods to solve surface structures as complicated as that of the Si(111) 7×7 . The first of these methods is maximum entropy combined with likelihood estimation, the second a combination of symbolic phasing methods and weakly interpolating modifications of the Sayre equation. These techniques are applied to two different elements of the structure determination, namely ab initio structure determination solely from diffraction intensity data and phase extension from a set of known phases derived from high resolution images. © 1997 Elsevier Science B.V.

Keywords: Adatoms; Electron–solid interactions, scattering, diffraction; High index single crystal surfaces; Single crystal surfaces; Surface relaxation and reconstruction; Transmission high-energy electron diffraction

1. Introduction

A long-standing problem in surface science has been to determine surface structures. One classic example of this is the Si(111) 7×7 surface which remained completely unsolved for many years until a model was proposed based upon the analysis of the Patterson function from electron diffraction data [1,2]. For the related question of structure determination of bulk crystals, one of the standard techniques to employ would appear to be “direct methods” which are now used to solve over 60% of crystal structures from single crystal X-ray diffraction data. (For further details of the method see Refs. [3–5].) In essence, these exploit probabi-

listic relationships arising from the fact that diffraction (with a kinematical approximation) occurs from atoms which can be considered uniformly and randomly distributed in the unit cell or, in the related Sayre methods, that the density and its square have the same features.

If it were possible to do the same for surface structures, determining these could become as relatively trivial as the solution of crystal structures from X-ray data. While we have recently demonstrated that it is possible to achieve this for a rather simple structure of gold on silicon [6,7], it does not follow that one can achieve the same success for much more complicated structures such as Si(111) 7×7 .

To see why this should be the case, some background on what information is available in such diffraction measurements, either X-ray or transmission electron diffraction, is appropriate. (With

* Corresponding author. E-mail: chris@chem.gla.ac.uk

¹ Present address: Sandia National Laboratories, Albuquerque, NM 87185-1056, USA.

symmetry averaging, transmission electron diffraction patterns from surfaces can be approximated relatively well using kinematical theory; see e.g. Refs. [8,9], although see also later.) Because bulk diffraction takes place simultaneously with the surface diffraction, one can only reliably measure those surface reflections which do not fall on the surface 1×1 lattice. In the case of electron diffraction one may also not be able to measure reflections very close to any of the bulk diffracted beams due to the plasmon inelastic background around them [10].

The surface of interest may be very different from the underlying bulk, or only a relatively small perturbation of the bulk structure. In the former case the unmeasured reflections may not be very substantial, in which case it should be possible to employ direct methods. However, in the latter case a large amount of the information is not available, so direct or Patterson methods may not work in any simple form. Conventional direct methods extrapolate and refine phases from either a small basis set or use a larger set with random initial phases, and will work only if the data set is complete, free from large systematic errors in the diffraction intensities, and if the structure is not too large (i.e. not more than ca. 100–150 non-hydrogen atoms in the asymmetric unit); if it is very incomplete (i.e. it does not fully span reciprocal space at ca. 1.1–1.2 Å resolution) and with large intensity errors, such as those arising from dynamical scattering, double diffraction of surface beams by the bulk and subsurface strains [11,12] and measurement errors, one needs alternative methods that overcome these limitations. A further complication is knowledge of the contents of the unit cell, which is rarely known at all accurately for surfaces, but fortunately, direct methods are relatively insensitive to uncertainties in cell contents.

The importance of the unmeasured reflections merits some emphasis. To put this into perspective, for the case of the Si(111) 7×7 surface the (7,7) reflections lie underneath the bulk (220) spots, and are the strongest ones for the surface at about 1.5–2.0 times the intensity of any other. As a consequence, even with correct phasing of all the measured intensities, the measured surface poten-

tial (for electrons, surface charge density with X-rays) will contain negative regions – the measured potential is the difference between a bulk structure and the surface, not a structure in its own right. Furthermore, not all the atoms in the structure may ever be visible in the correct potential; for instance, except for the dimers the atoms in the third layer of Si(111) 7×7 are only slightly displaced from their bulk positions and are essentially invisible. (They will show only as positive/negative dipoles.) If the unmeasured reflections are small, it should be possible to determine atomic positions and possibly even local charge densities relatively accurately; if they are not, the best that can reasonably be achieved is sufficient information about the primary framework from which, using classical Fourier methods, the whole structure can be determined.

We will show here that despite the above complications, it is possible to use existing direct methods formalisms in modified form such that even structures as complicated as Si(111) 7×7 can indeed be solved. The first of these is maximum entropy (ME) coupled with likelihood evaluation, where the constraints of positivity and entropy in real space both provide phase extrapolation and at the same time provide a probabilistic method that abandons the concept of uniform and randomly distributed atoms in the unit cell. The second uses a method of estimating the incompleteness of the data set coupled with symbolic methods and weakly interpolating modifications to the Sayre equation. These methods are applied to two different elements of the structure determination, namely ab initio structure determination solely from the diffraction intensity data and phase extension from a set of known phases derived from high resolution electron microscopy.

The structure of this paper is as follows: after very briefly reviewing the experimental data, the ME method is described, followed by an explanation of the weakly interpolative modifications of the Sayre equation. We then discuss the results obtained by both classes of approach for ab initio solutions of the Si(111) 7×7 structure. Finally, results of both approaches for phase extension are presented, followed by a final discussion.

2. Experimental method

The details of the measurement of the electron diffraction intensities have been described previously [9] and will not be repeated here. For the phase extension work, we used as the starting point phases from high-resolution electron micrograph images which contained information (at close to the Schertzer defocus) to about a resolution of 2.5 Å; details of which are described elsewhere [13].

3. Numerical methods

3.1. The maximum entropy method

We follow here a formalism developed by Bricogne [14–18]. This approach phases a set of unitary structure factor magnitudes $|U_{\underline{h}}|^{\text{obs}}$ which are derived from the intensity data by standard normalisation procedures:

$$(|U_{\underline{h}}|^{\text{obs}})^2 = k\sigma_2(|F_{\underline{h}}|^{\text{obs}})^2/\sigma_1 \sum_{j=1}^N f_j^2 \exp(-2B \sin^2 \theta/\lambda^2), \quad (1)$$

where B is an overall, isotropic temperature factor, k a scale factor (both obtained by a Wilson plot), f_j is the electron scattering factor for atom j , the summation spans the N atoms in the unit cell, θ is the Bragg angle for radiation of wavelength λ and

$$\sigma_n = \sum_{j=1}^N z(\text{eff})_j^n, \quad (2)$$

where $z(\text{eff})_j$ is the effective atomic number of atom j . Each U magnitude has an associated phase angle $\phi_{\underline{h}}$ which is to be determined. Because of rules of origin and enantiomorph definition, some phases $\phi_{\underline{h}}$ can usually (but not always – it depends on the space or plane group) be assigned, subject to standard rules, as a starting point in phase determination. Those reflections which are phased comprise the basis set $\{H\}$; the much larger disjoint set, the non-basis set, of unphased but experimentally measured amplitudes is $\{K\}$. There is a further set $\{U\}$, disjoint to both $\{H\}$ and $\{K\}$,

of the reflections which are unmeasured or otherwise discarded from the measured set. In surface diffraction this set comprises the bulk reflections from the 1×1 cell. Set $\{H\}$ can also be derived from the Fourier transform of the relatively low resolution image data. In the work presented here, both definitions of $\{H\}$ are used.

The phased reflections are used as constraints in an entropy maximisation where the relative entropy, S , is defined as:

$$S = - \int_V q(\underline{x}) \log [q(\underline{x})/m(\underline{x})] d^3\underline{x} \quad (3)$$

(where V is the unit cell volume, and $m(\underline{x})$ is the prior – in this case assumed uniform i.e. $m(\underline{x}) = 1/V$). The maximisation of S generates a map $q^{\text{ME}}(\underline{x})$ which satisfies the following conditions:

- (1) It is optimally unbiased i.e. it has maximum entropy.
- (2) Its Fourier transform reproduces the constraints (i.e. the U magnitudes and their associated phases) to within experimental error.
- (3) The Fourier transform of $q^{\text{ME}}(\underline{x})$ generates estimates of amplitudes and phases for non-basis set reflections in $\{K\}$ and $\{U\}$ via extrapolation. This is the process of ME extrapolation.

(2) and (3) are demonstrated diagrammatically in Fig. 1.

At this stage when only the origin (and enantiomorph, if relevant) reflections have been assigned phases, the extrapolation is weak, and the structure is not solved unless it is very small. If a larger basis set has been employed, the extrapolation process at this point may well be sufficient to give at least a partial structure. In the former case, unphased reflections are added to the starting set

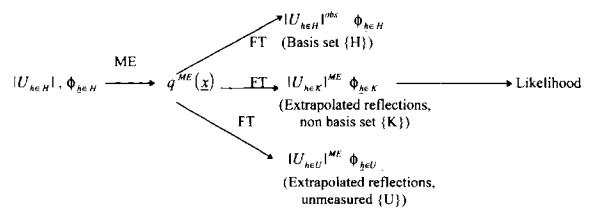


Fig. 1. Extrapolation via maximum entropy.

with permuted phases giving rise to a multisolution environment just as in conventional direct methods. To do this the current basis set is chosen and a few reflections with large associated U magnitude which optimally enlarge the second neighborhood of the basis set are selected. (The second neighborhood is defined by reflections $\mathbf{h}_1 \pm {}^t\mathbf{R}_g \cdot \mathbf{h}_2$ for $\mathbf{h}_1, \mathbf{h}_2 \in \mathbf{H}$, where ${}^t\mathbf{R}_g$ is the transpose of a rotation matrix obtained from the crystal space or plane group.) For centric reflections, which is the case throughout this study, both possible values of the phase angle are used i.e. $0, \pi$; alternatively, this can be described in terms of signs + or - respectively. A constrained entropy maximisation for each possible phase permutation is now carried out. Judging which phase sets are the most probable is done using likelihood estimation, employing a suitable likelihood function in its diagonal form in which the extrapolates are decoupled and treated as independent [14–17].

In this case, for each centric extrapolated, non-basis set reflection \underline{k} the likelihood measure, in its diagonal approximation, can be written:

$$\begin{aligned} A_{\underline{k}} &= \frac{2|U_{\underline{k}}|^{\text{obs}}}{\pi(2\epsilon_{\underline{k}}\Sigma + \sigma_{\underline{k}}^2)} \\ &\exp \left\{ -\frac{1}{2} \frac{(|U_{\underline{k}}|^{\text{obs}})^2 + |U_{\underline{k}}^{\text{ME}}|^2}{2\epsilon_{\underline{k}}\Sigma + \sigma_{\underline{k}}^2} \right\} \cosh \left(\frac{|U_{\underline{k}}|^{\text{obs}}|U_{\underline{k}}^{\text{ME}}|}{2\epsilon_{\underline{k}}\Sigma + \sigma_{\underline{k}}^2} \right) \end{aligned} \quad (4)$$

where $\underline{k} \in K$, $\sigma_{\underline{k}}^2$ is the variance of $|U_{\underline{k}}|^{\text{obs}}$, Σ is a refinable measure of unit cell contents ($\Sigma \approx 1/2N$) and $\epsilon_{\underline{k}}$ is the statistical weight. This is a Rice distribution comprising a Gaussian exponential term with a hyperbolic cosine offset. Note also that this expression is a measure of agreement between $|U_{\underline{k}}|^{\text{obs}}$ and $|U_{\underline{k}}^{\text{ME}}|$, having a maximum value when $|U_{\underline{k}}|^{\text{obs}} = |U_{\underline{k}}^{\text{ME}}|$. As in traditional likelihood analysis, a corresponding null hypothesis is defined for the situation of zero extrapolation, $|U_{\underline{k}}^{\text{ME}}| = 0$, which gives the Gaussian distribution of Wilson statistics. For centric reflections:

$$A_{\underline{k}}^0 = \frac{2|U_{\underline{k}}|^{\text{obs}}}{\pi(\epsilon_{\underline{k}}\Sigma + \sigma_{\underline{k}}^2)} \exp \left\{ -\frac{1}{2} \frac{(|U_{\underline{k}}|^{\text{obs}})^2}{2\epsilon_{\underline{k}}\Sigma + \sigma_{\underline{k}}^2} \right\}. \quad (5)$$

We now define:

$$L_{\underline{k}} = \log \frac{A_{\underline{k}}}{A_{\underline{k}}^0}. \quad (6)$$

The global log-likelihood gain (LLG) for node n is then:

$$\text{LLG}_n = \sum_{\underline{k}} L_{\underline{k}}. \quad (7)$$

The LLG will be largest when the phase assumptions for the corresponding basis set lead to predictions of amplitudes of the unphased reflections which best agree with the observed intensity measurements for the non-basis set reflections, and in this context it is a powerful figure of merit. However, rather than just choose those phase sets with high associated LLG, which is a somewhat subjective process, tests of significance are used. The LLGs are analysed for phase indications using the t -test [19] which defines the level of significance of the difference between two means. The simplest example involves the detection of the main effect associated with the sign of a single centric phase. The LLG average, μ^+ , and its associated variance V^+ is computed for those sets in which the sign of this permuted phase under test is +. The calculation is then repeated for those sets in which the same sign is - to give the corresponding μ^- , and variance V^- . The t -statistic is then:

$$t = |\mu^+ - \mu^-| / \sqrt{V^+ + V^-}. \quad (8)$$

The use of the t -test enables a sign choice to be derived with an associated significance level. This sort of calculation is repeated for all the single phase indications, and is then extended to combinations of two and three phases. In general, only relationships with associated significance levels $< 2\%$ are used, but this has to be relaxed with sparse diffraction data sets such as we have here. Each of the m phase relationships, i , so generated is given an associated weight w_i :

$$w_i = \left(1 - \frac{I_1(s_i)}{I_0(s_i)} \right), \quad (9)$$

where I_1 and I_0 are the appropriate Bessel functions and s_i is the significance level of the i th relationship from the t -test. This weighting function reflects the

need for a scheme in which the absolute values of the significance levels are not given undue emphasis since they are themselves subject to errors arising from the nature of the likelihood function used and the lack of error estimates for the LLGs themselves.

Each node n is now given a score, s_n :

$$s_n = \text{LLG}_n \sum_{j=1}^m w_j, \quad (10)$$

where the summation spans only those phase relationships where there is agreement between the basis set phases and the t -test derived phase relationships. The scores are sorted and only the top 8–16 nodes are kept; the rest are discarded. New reflections are now permuted and a corresponding new set of ME solutions is generated. In this way we build a phasing tree in which each phase choice is represented as a node, and has a score, or figure of merit, based on its log likelihood gain. The root node of the tree is defined by the origin defining reflections. The first set of phase permutations defines the second level. Those which do not pass the analysis of likelihood are discarded, then further phase permutations are used to generate the third level, and this continues until a recognisable structure or structural fragment appears.

$q^{\text{ME}}(\underline{x})$ is a probability distribution, and not a potential map in the traditional sense (although its peaks do correspond to atom positions). The trial potential maps generated in this approach are called centroid maps, and are computed as Sim filtered U maps [14–17]. In this situation the basis set reflections (amplitudes and phases) contribute to the map with full weight whereas the extrapolated reflections $\{K\}$ are given weights computed via:

$$|U_k|^{\text{obs}} \tanh(X_k) \exp(i\phi_k^{\text{ME}}), \quad (11)$$

with:

$$X_k = (N/\epsilon_k)|U_k|^{\text{obs}}|U_h^{\text{ME}}|. \quad (12)$$

Phase angles are those extrapolated from $q^{\text{ME}}(\underline{x})$. Unmeasured reflections may be included in these maps if required by using unit weights, and with both phase angles and U magnitudes extrapolated from $q^{\text{ME}}(\underline{x})$.

Finally, to allow for measurement errors, we do

not aim for a perfect fit between $|U_h|^{\text{obs}}$ and $|U_h^{\text{ME}}|$; rather, a reduced χ^2 statistic is used:

$$\chi^2 = \frac{1}{n} \sum_{h \in H} \frac{1}{\sigma_h^2} (|U_h|^{\text{obs}} - |U_h^{\text{ME}}|)^2, \quad (13)$$

where n is the total number of degrees of freedom which, in the centrosymmetric space group case which we have here, is the number of reflections. Overfitting can produce maps with spurious detail, whereas underfitting has the opposite effect as well as reducing the corresponding LLGs. In general, we aim at a target value of 1.0 for χ^2 , but for some data sets it is more appropriate to stop at the point of maximum likelihood which is the case here. It is worth noting at this juncture that the ME formalism, unlike traditional direct methods, is capable of using the standard deviations of the intensity measurements.

The above method has been described for the centrosymmetric case, but is equally valid for non-centrosymmetric plane and space groups. There are three major differences between the centrosymmetric and non-centrosymmetric cases:

(1) Quadrant permutation is used for permuting acentric phases (those which have no phase restrictions). In this case each unknown phase used for building the phasing tree takes four possible values: $\pm \pi/4, \pm 3\pi/4$.

(2) The likelihood functions are modified such that Eq. (4) employs the zero-order Bessel function I_0 instead of the cosh function and with a slightly modified argument [14, 15].

(3) Generally, there is a need to define an enantiomorph, but the relevant theory has long been defined in classical direct methods, and can readily pass over into the ME environment [4]. The computations are more time consuming because the phase trees are larger, but the same principles are used; indeed, in trials, the technique has solved non-centrosymmetric problems of all types. Equally the formalism is applicable without alteration to two-dimensional data sets: the underlying statistics are equally valid, and the procedures similar, although, in general, 2-D data is more difficult to phase accurately than 3-D.

The MICE computer program is a practical implementation of a part of the Bricogne formal-

ism [16,17]. Surveys of the method and its practical applications can be found in [20–23]. The use of this procedure for the ab initio structure determination of crystals consisting of organic molecules from electron diffraction data has also been described [24].

3.2. The Sayre equation

It is convenient to employ a slight change in nomenclature. The Sayre-based methods use the unitary structure factors $U(\mathbf{g})$, where \mathbf{g} is a reciprocal lattice vector of the reconstructed surface, which are numerically more convenient, corrected by a window function $W(\mathbf{g})$, i.e.:

$$U(\mathbf{g}) = W(\mathbf{g})F(\mathbf{g})/f(\mathbf{g}) \quad (14)$$

where $f(\mathbf{g})$ is the atomic scattering factor. The window, which is similar in function to Walsh and other windows for power-spectrum estimation, was chosen to satisfy approximately:

$$W(\mathbf{g}) = \sum_k W(\mathbf{g} - \mathbf{k})W(\mathbf{k}) \quad (15)$$

only for the range of measured \mathbf{g} values. In practice, the form:

$$W(\mathbf{g}) = \exp(-0.5\mathbf{g}^2/\mathbf{g}_{\max}^2) \quad (16)$$

with \mathbf{g}_{\max} the largest value used reduced the error to a few percent. In effect, this window reduces ringing in the potential due to truncation of the Fourier series.

The zero Fourier coefficient was estimated as equal to the sum of the squares of the experimental intensities, which empirically is rather close to the true value. (Note that unlike the bulk case, one can rarely if ever know how many atoms are in the unit cell.) New phases for the were extrapolated from the calculated phases $U_c(\mathbf{g})$ by equating them, which is equivalent to the classical tangent formula approach [25]. How good a fit was obtained was determined by a figure of merit (FOM):

$$R = \sum_{\mathbf{g}} |f(\mathbf{g})/[\sigma(\mathbf{g})W(\mathbf{g})]| [U(\mathbf{g}) - \alpha U_c(\mathbf{g})]^2 / \sum_{\mathbf{g}} \{f(\mathbf{g})U(\mathbf{g})/[\sigma(\mathbf{g})W(\mathbf{g})]\}^2 \quad (17)$$

where α is a scaling constant and $\sigma(\mathbf{g})$ the error for a given reflection. This is equivalent to deter-

mining the most likely value of the potential assuming normal errors in the experimental measurements. (We experimented with modifications of this form, e.g. ignoring the experimental errors or taking the moduli rather than the square. Including the errors did make a small but noticeable effect; with it the FOM is much more sensitive to the weaker intensities than without it. The importance of including the errors will be discussed later.)

All the calculations were performed using fast Fourier transforms, which, provided that appropriate care is taken to avoid aliasing, are faster than convolutions. One form is the classic Sayre equation, i.e. with r in real space:

$$U_c(r) = U(r)^2. \quad (18)$$

However, this form has no interpolative power. For a complete data set where the $U(r)$ is a set of delta functions for the correct solution, one can also use:

$$U_c(r) = U(r)^3 \quad (19)$$

$$= \exp[\text{const}^* U(r)] \quad (20)$$

$$= U(r)|U(r)|. \quad (21)$$

The first two of these contain triple products which have interpolations of the unmeasured intensities. The last is related to a Gerchberg restoration scheme (e.g. Ref. [26]), in the following sense. The measured $U(r)$ can be written as:

$$U(r) = T(r) - S(r) \quad (22)$$

where $T(r)$ is the complete unitary potential and $S(r)$ the missing part. The modulus of $U(r)$ is a partial restoration such that the potential is everywhere positive, and is approximately:

$$|U(r)| \sim T(r) + S(r). \quad (23)$$

Hence:

$$U(r)|U(r)| \sim T(r)^2 - S(r)^2. \quad (24)$$

An alternative is to project $|U(r)|$ back to the Fourier domain and only include the unmeasured amplitudes, but, in practice, Eq. (21) seems to be just as effective and rather faster.

Eqs. (19) and (20) and Eq. (21) as well as the Sayre equation itself were used in this study. Just as in the ME case, a three-dimensional formalism

has been presented here, but it has an equal validity in the 2-D environment, although phasing becomes more difficult, because there are fewer terms on the right-hand side of the Syre equation in whatever form it is presented. It should also be noted that while the forms of these equations can interpolate the unknown values, there is no guarantee that they are stable. We will return to this point below.

4. Ab initio solutions

The diffraction data listed were normalised using MITHRIL [27,28] to give the unitary structure magnitudes ($|U_h|^{obs}$) and their associated standard deviations using electron scattering factors; the overall isotropic temperature factor B was calculated to be -0.58 \AA^2 which is physically impossible. This is common with incomplete data sets of this type; it arises from data incompleteness, the multiple scattering effects in the data (primarily double diffraction by the silicon substrate), subsurface strains [11,12] and from measurement errors. Accordingly an overall temperature factor of zero was imposed for the ME calculations, while a value of 1.5–2.0 times that for bulk Si was used for the Sayre methods (the results were not sensitive to the exact value). The plane group used was P6mm. The number of independent input reflections was 193. The U magnitudes, their associated standard deviations and their resolution in \AA are tabulated in Table 1.

4.1. Method I: maximum entropy

Ab initio phasing was rather difficult. Using the full data set and despite many attempts, no truly workable maps could be generated: they all required knowledge of the answer to be correctly interpreted. It was then decided to work in resolution ranges. The intensity data extend to ca. 0.6 \AA , and very high resolution data of this sort can have large systematic errors associated with it, and, of course, the bulk reflections have been removed. Under these circumstances it is often best to work with a sub-set of reflections at relatively low resolution, and phase these first, thus

generating a structural envelope which is then used to phase higher resolution data.

Accordingly, the following procedure was used:

(1) The full data set was normalised as before.

(2) In this plane group with the bulk reflections removed, there are no available reflections for origin definition. This poses no particular problems: a set of six reflections at maximum resolution of 2 \AA was selected on the grounds of optimal second neighborhood definition. To do this it is assumed that all the reflections are present in the basis set, and those least connected to this set by their second neighborhood are removed one by one until the required number of reflections is left. The reflections chosen were 96(8, -4), 58(6,0), 60(7, -1), 39(9, -2), 26(8,0) and 43(8, -1). The phases were given permuted values in a full factorial design, thus generating a first level of $2^6 = 64$ nodes. Coincidentally, all these reflections had phase angles available from image data (although this phase data were not used here).

Each node was subjected to constrained entropy maximisation, and the set of 64 nodes analysed as described previously using t -tests and scores. The iterative entropy maximisation routines were stopped at points of maximum LLG for each node. This corresponded to χ^2 values lying between 2.0 and 14.9. The phasing tree thus generated is summarised in Table 2. The node with the highest score was number 43 which also had a zero basis set phase error when measured against the image derived phases. A centroid potential map for node 43, however, did not reveal the complete structure, and so a second level of the phasing tree was constructed by:

(1) Increasing the basis set resolution to 1 \AA .

(2) Taking the top ranked eight nodes from level 1 of the tree.

(3) Permuting the phases of reflections 6(14, -1), 7(15, -4), 9(10, -3), 12(14, -4), 19(14, -2), 22(14, -5) and 23(14, -3), thus generating $8 \times 2^7 = 1024$ new nodes.

Each node was subjected to constrained entropy maximisation as before, and the scores analysed as for level 1. Three nodes had scores that were considerably in excess of any others. Centroid maps with extrapolation down to 0.6 \AA were generated for all three. The unmeasured reflections $\{U\}$,

Table 1

The intensity data in the form serial number, h , k , $|U_h^{\text{obs}}|$ with its esd in brackets and the resolution, d , in Å

No.	h	k	$U(\text{esd})$	$d(\text{\AA})$	No.	h	k	$U(\text{esd})$	$d(\text{\AA})$
1	24	-10	0.240(44)	0.79	52	26	-12	0.115(33)	0.73
2	31	-14	0.234(88)	0.61	53	24	-4	0.115(25)	0.74
3	13	0	0.228(12)	1.27	54	27	-11	0.112(24)	0.70
4	21	-6	0.216(23)	0.88	55	28	-13	0.112(35)	0.68
5	27	-6	0.214(33)	0.67	56	20	-2	0.111(22)	0.86
6	14	-1	0.205(11)	1.22	57	28	-10	0.110(23)	0.67
7	15	-4	0.202(10)	1.22	58*	6	0	0.109(2)	2.74
8	17	-7	0.201(18)	1.11	59	25	-12	0.109(17)	0.76
9*	10	-3	0.200(6)	1.85	60*	7	-1	0.108(7)	2.51
10	31	-13	0.199(56)	0.61	61	18	-8	0.105(22)	1.05
11	24	-7	0.195(47)	0.77	62	16	-5	0.105(12)	1.16
12	14	-4	0.193(7)	1.32	63	17	-4	0.103(18)	1.07
13	23	-9	0.193(16)	0.82	64	24	-11	0.102(24)	0.79
14	29	-11	0.187(53)	0.65	65	20	-6	0.101(19)	0.93
15	31	-11	0.175(53)	0.60	66	16	-4	0.101(12)	1.14
16	22	-8	0.173(14)	0.85	67	17	-5	0.098(11)	1.09
17	21	-3	0.173(38)	0.84	68	24	-8	0.098(34)	0.78
18	21	-4	0.173(23)	0.85	69*	9	0	0.097(4)	1.83
19	14	-2	0.167(16)	1.26	70	20	-1	0.097(13)	0.84
20	17	0	0.165(29)	0.97	71	30	-9	0.097(38)	0.62
21	21	-5	0.163(18)	0.87	72*	11	0	0.097(16)	1.50
22	14	-5	0.161(8)	1.34	73	24	-12	0.096(23)	0.79
23	14	-3	0.159(23)	1.29	74	15	-5	0.094(11)	1.24
24	21	-2	0.153(17)	0.82	75*	11	-3	0.093(7)	1.67
25	21	-10	0.150(22)	0.90	76	16	0	0.092(11)	1.03
26*	8	0	0.149(11)	2.06	77	28	-11	0.092(19)	0.67
27	22	-4	0.147(37)	0.81	78	21	-8	0.090(23)	0.90
28	29	-7	0.145(46)	0.63	79	25	-10	0.088(28)	0.76
29	22	-11	0.145(16)	0.86	80	24	-9	0.087(30)	0.78
30	27	-7	0.143(21)	0.68	81	27	-12	0.087(16)	0.70
31	27	-13	0.140(24)	0.70	82	28	-12	0.086(28)	0.68
32	20	-7	0.138(18)	0.94	83	19	-1	0.085(24)	0.89
33	17	-6	0.131(26)	1.10	84	18	-7	0.084(46)	1.05
34	26	-5	0.131(25)	0.69	85*	12	-6	0.084(8)	1.58
35	25	-4	0.130(24)	0.71	86	25	-11	0.082(38)	0.76
36	12	0	0.130(7)	1.37	87	18	-9	0.081(14)	1.06
37	25	-7	0.128(52)	0.74	88*	11	-5	0.080(9)	1.73
38	28	-8	0.127(26)	0.66	89	28	-9	0.078(21)	0.66
39*	9	-2	0.127(5)	2.01	90	13	-4	0.077(7)	1.43
40	27	-10	0.126(34)	0.70	91	17	-3	0.077(12)	1.05
41	18	-4	0.126(30)	1.01	92	23	-7	0.077(12)	0.81
42	24	-5	0.121(20)	0.75	93	25	-6	0.076(22)	0.73
43*	8	-1	0.121(6)	2.18	94	26	-11	0.076(17)	0.73
44	15	0	0.120(15)	1.10	95	16	-7	0.075(12)	1.19
45	30	-14	0.119(26)	0.63	96*	8	-4	0.074(2)	2.38
46	22	-7	0.118(12)	0.85	97	20	-3	0.073(15)	0.88
47	24	-6	0.117(21)	0.76	98	20	-9	0.073(14)	0.95
48	26	-13	0.117(7)	0.73	99	15	-1	0.073(12)	1.13
49	18	0	0.117(37)	0.91	100	13	-3	0.071(5)	1.40
50	23	-11	0.117(19)	0.83	101	26	-6	0.071(29)	0.70
51	29	-8	0.116(77)	0.63	102	16	-6	0.069(16)	1.18

Table 1 (continued)

The intensity data in the form serial number, h , k , $|U_h^{\text{obs}}|$ with its esd in brackets and the resolution, d , in Å

No.	h	k	$U(\text{esd})$	$d(\text{\AA})$	No.	h	k	$U(\text{esd})$	$d(\text{\AA})$
103	18	-1	0.069(25)	0.94	149	19	-5	0.041(11)	0.97
104	19	-6	0.068(8)	0.98	150	30	-10	0.040(121)	0.62
105	10	-1	0.066(4)	1.73	151	29	-13	0.040(105)	0.65
106	21	-9	0.065(13)	0.90	152*	11	-1	0.039(13)	1.56
107	23	-6	0.065(24)	0.80	153	22	-9	0.039(19)	0.86
108	23	-4	0.064(19)	0.77	154*	5	0	0.039(2)	3.29
109	20	-5	0.064(14)	0.91	155*	9	-3	0.037(5)	2.07
110	19	-8	0.064(12)	1.00	156	19	-4	0.037(17)	0.95
111	20	-8	0.063(14)	0.94	157	22	-6	0.037(55)	0.84
112	26	-8	0.063(18)	0.71	158	22	-5	0.036(32)	0.82
113	13	-1	0.063(6)	1.31	159	18	-2	0.036(14)	0.96
114*	10	-2	0.063(6)	1.80	160*	4	-1	0.036(3)	4.57
115	27	-9	0.062(59)	0.69	161	23	-10	0.035(37)	0.82
116	29	-12	0.060(50)	0.65	162	16	-2	0.034(8)	1.09
117	19	-7	0.060(18)	0.99	163*	7	-2	0.034(3)	2.64
118	30	-13	0.060(71)	0.63	164	19	-3	0.033(15)	0.93
119	20	-10	0.059(13)	0.95	165	23	-8	0.032(38)	0.81
120*	10	0	0.059(18)	1.65	166	16	-3	0.032(15)	1.12
121	23	-3	0.058(30)	0.76	167	17	-2	0.032(17)	1.02
122	25	-9	0.058(24)	0.75	168*	8	-3	0.031(5)	2.35
123	12	-1	0.057(6)	1.43	169	22	-2	0.031(48)	0.78
124	22	-10	0.057(17)	0.86	170	16	-8	0.030(10)	1.19
125	26	-10	0.057(33)	0.72	171	19	-2	0.029(29)	0.91
126*	11	-2	0.056(8)	1.62	172*	11	-4	0.028(7)	1.71
127	17	-8	0.056(12)	1.12	173	17	-1	0.028(18)	1.00
128	13	-2	0.055(6)	1.36	174*	10	-4	0.027(7)	1.89
129	18	-6	0.055(11)	1.04	175	15	-3	0.027(10)	1.20
130	18	-3	0.054(21)	0.99	176*	4	-2	0.026(1)	4.75
131	23	-5	0.053(19)	0.79	177	16	-1	0.025(30)	1.06
132	20	-4	0.053(12)	0.90	178	30	-15	0.025(138)	0.63
133	26	-9	0.052(20)	0.72	179*	12	-3	0.023(9)	1.52
134*	9	-4	0.052(5)	2.11	180*	9	-1	0.022(4)	1.93
135	29	-10	0.052(47)	0.65	181	15	-6	0.021(47)	1.26
136	18	-5	0.051(9)	1.02	182	15	-2	0.021(16)	1.17
137	19	0	0.051(14)	0.87	183	12	-2	0.020(23)	1.48
138*	3	0	0.051(2)	5.49	184*	10	-5	0.020(5)	1.90
139	13	-5	0.050(7)	1.45	185*	4	0	0.020(5)	4.12
140*	12	-4	0.050(13)	1.56	186*	6	-3	0.016(3)	3.17
141	27	-8	0.050(62)	0.69	187*	6	-1	0.015(18)	2.96
142	25	-8	0.049(64)	0.74	188*	7	-3	0.015(18)	2.71
143	25	-5	0.048(30)	0.72	189*	5	-2	0.012(12)	3.78
144	19	-9	0.048(12)	1.00	190*	3	-1	0.011(88)	6.22
145*	12	-5	0.048(6)	1.58	191*	8	-2	0.009(41)	2.28
146	26	-7	0.048(38)	0.71	192*	6	-2	0.008(31)	3.11
147	29	-9	0.045(100)	0.64	193*	5	-1	0.008(15)	3.59
148	22	-3	0.043(20)	0.80					

*Signifies a reflection for which phase information is available via the Fourier transform of a suitable electron microscope image.

Table 2

The first level of the maximum entropy-likelihood phasing tree at 2 Å^a

Node	Entropy	Σ	LLG	Node	Entropy	Σ	LLG
1	-0.351	0.00085	1.42	33	-0.348	0.00283	-0.91
2	-0.327	0.00247	-0.16	34	-0.307	0.00198	0.58
3	-0.250	0.00217	-0.17	35	-0.241	0.00268	-0.28
4	-0.228	0.00265	-0.58	36	-0.228	0.00179	-0.09
5	-0.275	0.00209	0.03	37	-0.276	0.00160	0.81
6	-0.245	0.00144	1.03	38	-0.242	0.00232	-0.03
7	-0.260	0.00194	0.28	39	-0.287	0.00115	1.31
8	-0.233	0.00144	1.22	40	-0.231	0.00240	0.07
9	-0.249	0.00239	-0.16	41	-0.239	0.00164	0.77
10	-0.257	0.00153	0.96	42	-0.254	0.00212	0.16
11	-0.264	0.00221	0.17	43	-0.286	0.00107	1.78
12	-0.252	0.00139	1.25	44	-0.252	0.00215	-0.23
13	-0.299	0.00114	0.35	45	-0.274	0.00226	-0.40
14	-0.292	0.00254	-0.61	46	-0.283	0.00215	-0.74
15	-0.267	0.00083	0.74	47	-0.261	0.00256	-0.93
16	-0.224	0.00239	-0.08	48	-0.212	0.00185	0.28
17	-0.326	0.00108	1.67	49	-0.324	0.00213	0.15
18	-0.314	0.00213	0.11	50	-0.309	0.00126	-1.07
19	-0.236	0.00123	1.21	51	-0.229	0.00241	-0.85
20	-0.230	0.00227	0.03	52	-0.221	0.00193	-0.31
21	-0.237	0.00255	-0.13	53	-0.244	0.00173	0.56
22	-0.234	0.00186	0.47	54	-0.229	0.00219	-0.19
23	-0.246	0.00248	-0.18	55	-0.246	0.00140	0.99
24	-0.234	0.00179	0.53	56	-0.218	0.00230	-0.23
25	-0.224	0.00239	-0.22	57	-0.252	0.00156	0.57
26	-0.243	0.00185	0.53	58	-0.228	0.00247	-0.40
27	-0.241	0.00253	-0.27	59	-0.248	0.00158	0.67
28	-0.244	0.00167	0.61	60	-0.250	0.00241	-0.13
29	-0.295	0.00209	-0.19	61	-0.269	0.00228	-0.69
30	-0.255	0.00208	-0.17	62	-0.254	0.00120	-0.80
31	-0.218	0.00111	1.45	63	-0.225	0.00226	0.01
32	-0.217	0.00185	-0.17	64	-0.223	0.00053	-1.34

^aThe columns are the node number, the entropy, the refined Σ parameter and the log-likelihood gain associated with that node

including the bulk data, were not included; their presence made very little difference to the final map.

The best map is shown in Fig. 2a; the map quality is high: there is a missing dimer atom, but it is weakly indicated by the trefoil shape of the adjacent adatom; there is an annulus around the origin and peak heights are a little uneven, but it is a straightforward matter to complete this structure by conventional Fourier methods. As mentioned earlier, one should not expect to see all the atoms when the strongest reflections are missing from the data set, indeed classical direct methods

applied to single crystal diffraction data rarely reveal the entire structure. The remaining two maps were very similar, and one of them is shown in Fig. 2(b). The large peaks are in the correct place, but there is spurious detail and the electron density is concentrated in one region of the cell. Nonetheless, the structure can be completed from these maps. For reference, Fig. 3 shows the accepted structure of the reconstructed surface.

The maps are projections from two-dimensional data, and carry no information about atomic positions normal to the surface. In principle this could be generated by incorporating information along

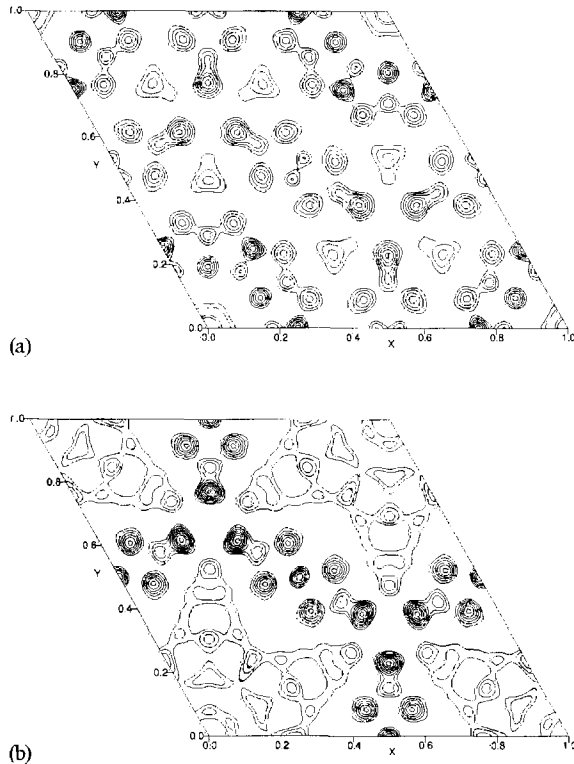


Fig. 2. (a) The best centroid potential map from the ME ab initio phase determination. (b) A typical solution with high likelihood and score, but with higher phase errors than Fig. 2a. Both maps extrapolate to 0.6 Å, and are capable, with the application of Fourier methods, of yielding the complete structure.

the rel-rods for X-ray diffraction. In general, one can infer the approximate positions from modeling arguments. In fact, the information provided by two-dimensional diffraction is precisely that which is difficult to extract from a standard LEED I(V) analysis which is, in contrast, very good at fitting distances normal to the surface, but very bad at fitting parallel distances.

However, any attempts to extend direct phasing below 1 Å using ME methods and the phasing tree already generated were wholly unsuccessful as evidenced by falling LLGs, which is always a sign of problems, and potential maps that contained a great deal of spurious detail. In addition to both statistical and systematic errors in the data, as the resolution is increased the number of undetermined intensities also increases, playing a major role in accumulating phase errors. Nonetheless the ME

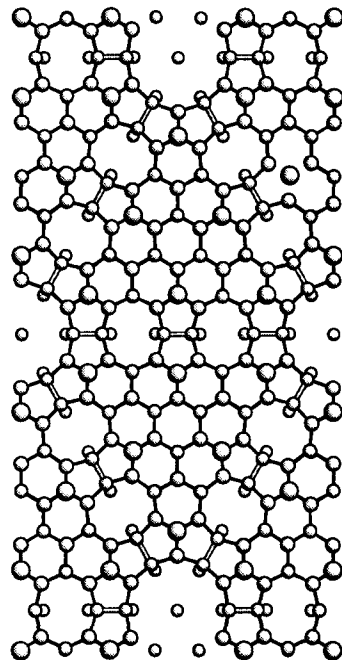


Fig. 3. The structure of the Si(111) 7×7 surface.

method has successfully, and quite routinely, solved a complex surface structure.

The calculation itself took less than 30 min on a laboratory network of UNIX workstations in which the nodes were passed from a central server to a total of 15 available processors. This is a great benefit of the computational side of the ME formalism – it lends itself readily to this simple coarse-grained form of parallelisation.

4.2. Method II: symbolic analysis with weakly interpolative methods

Since ME works, one might think that conventional direct methods might also give the solution. However, applying various different combinatorial methods with as many as 20 different basis set reflections (using a genetic algorithm [29,30]) at different resolutions, we could not obtain the same solution; visually, the best solutions, as ranked by the figure of merit, were often unphysical. This is probably a consequence of incomplete data, the missing bulk reflections and the very regular (non random) nature of the structure – all problems to

which the ME method is less susceptible. Although the known solution was often one of the better (in terms of the FOM) results, there was no way of objectively picking it out. This was true not just for the Sayre equation, but also for the other methods in Eqs. (19)–(21). The key is that these methods do not adequately interpolate the unknown intensities which, as will be shown below, are strong.

There is another approach, based on traditional methods, at the heart of which is an inductive test that can be applied to determine whether the data set is complete, or very incomplete based around triplets and the related sigma-1 relationships [4]. Let us suppose that the data is very incomplete, and there are strong surface reflections buried under the 1×1 bulk reflections. Denoting the 1×1 family as f , it follows that there must exist a good number of strong surface reflections p and q such that there is a triplet of the form $p+q=f$. Conversely, if the unmeasured 1×1 intensities have only a small surface contribution, it follows that there will be few if any such relationships. Thus one can deduce whether the family of 1×1 reflections is weak or strong.

As an example, for the Au on Si(111) surface [6,31] the strongest reflections are the (2, 1) and (1, 2) in the space group p31m (see Figure 1 in Ref. [31]). This implies that (1, 1) may be substantial, but the bulk reflection (3, 0) {=bulk (220)} is not. From the general structure of the diffraction pattern, there are relatively few combinations which can lead to (1, 1), so by inference the data is relatively complete.

Applying this to the Si(111) 7×7 surface, by inspection the (7, 7) reflections {=bulk (220)} must be strong. A weaker case can also be made that the (7, 0) reflections should be fairly strong. Furthermore, most of these are simple triplet relationships between two different symmetry related reflections, for instance (7, 1), (7, 2) and (7, 3). Within the space group p6mm each of these can only have a phase of π or $0 (=2\pi)$, which implies that the phase of (7, 7) is 2π . This is an example of the sigma-1 relationship which also used in conventional direct methods [4].

Developing the symbolic method further, one can then imply that the phases, ϕ , of strong beams

connected by (7, 7) must be the same, which gives:

$$\phi(6, 1) = \phi(8, 0), \quad (25)$$

$$\phi(7, 1) = \phi(0, 6), \quad (26)$$

all of which are strong reflections. Finally, the strong reflection (0, 13) is connected by symmetry equivalents of (6, 1) and (7, 3), similar to (7, 7), and also by the combination of (7, 7) and (6, 1). Since the symmetry equivalents give a phase of 2π , and we already know that (7, 7) has a phase of 2π , we can infer that:

$$\phi(6, 1) = \phi(8, 0) = \phi(0, 13) = 2\pi. \quad (27)$$

This now provides almost enough information to produce a potential map that solves the structure. Scanning over 2^{10} permutations of the strongest ten unphased reflections using the Sayre equation and Eqs. (19)–(21), the FOM's were sorted and the best solutions based on the lowest FOM were analyzed at different resolution levels. Originally we excluded the measurement error term in Eq. (17); in this case the conventional Sayre/tangent formula did not work at any resolution, while the others did when the resolution was limited to 2.8 \AA . With the measurement error included, the best solutions for all the models at a resolution of 2.8 \AA was of high quality, as shown in Fig. 4. However, only the best Sayre solution was good – the next three solutions were not, while all the top solutions of the other approaches were very similar. At higher resolutions, the Sayre

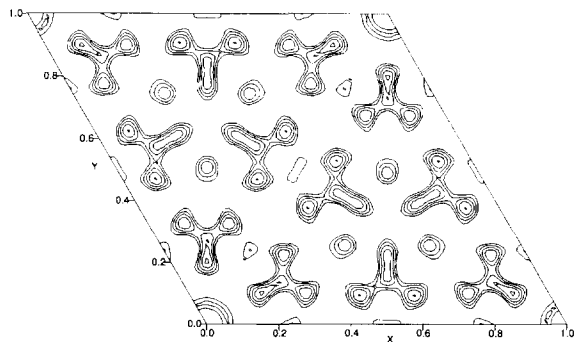


Fig. 4. The best ab initio solution of the Si(111) 7×7 surface using Sayre and related methods. The data resolution is 2.8 \AA .

method was unviable whereas the other approaches still gave rather good results. The resulting maps are not as clean as the ME derived ones: they have lower resolution and less detail, but they represent a viable model of the surface structure at 2.8 Å.

5. Phase extension

5.1. Method I: maximum entropy

A total of 41 unique phases were available from image Fourier transform studies of high resolution images [13]. We excluded the (7, 0) reflection which were available from the images but not in the diffraction data. The maximum resolution of these reflections was ca. 1.5 Å. They are marked with an asterisk (*) in Table 1. Most of them have very weak associated U magnitudes. A U map calculated before any entropy maximisation is shown in Fig. 5. The general features of the surface structure are present although there is some spurious detail and some peaks are absent or coalesced. There is insufficient detail to consider the structure characterised at the atomic level, especially when the (7, 0) reflection is omitted. Accordingly, the 41 reflections were used as a basis set and subjected to entropy maximisation without recourse to any tree-building phasing methods. The iterative entropy maximisation algorithm was stopped at the point of maximum likelihood. The LLG was

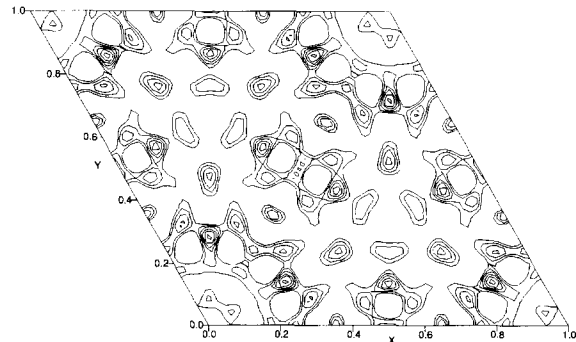


Fig. 5. A U map based on 41 image-derived phased reflections. The maximum resolution is 1.5 Å.

2.42. The calculation took less than 1 min on a SUN Sparc-20 workstation.

The resulting centroid potential map is shown in Fig. 6a with a resolution of 0.6 Å. The whole structure is clearly delineated.

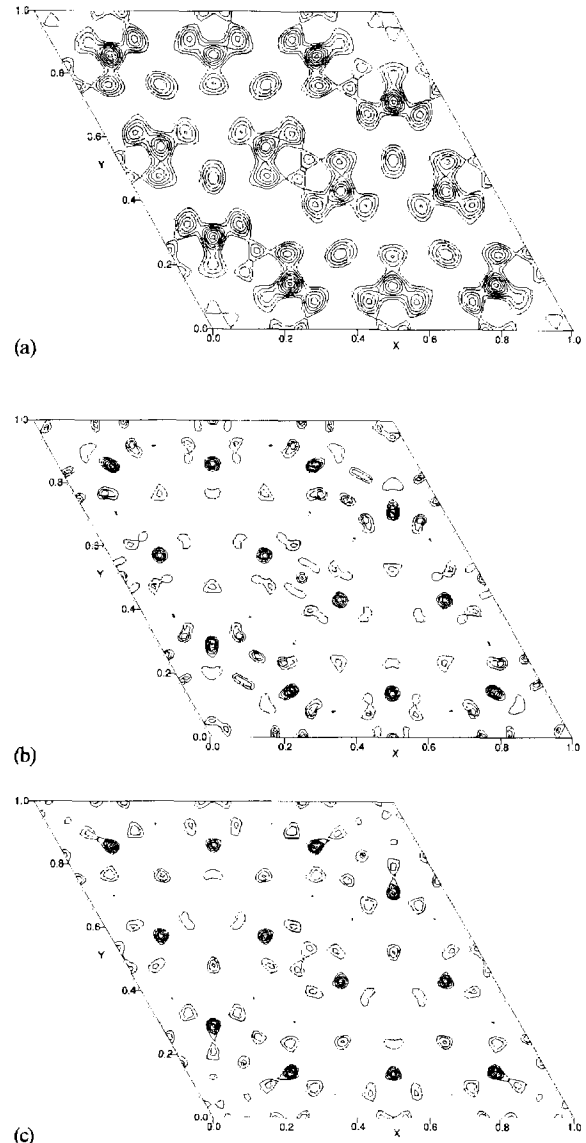


Fig. 6. (a) A centroid potential map derived from entropy maximisation of the image basis set used in Fig. 5 (b) A potential map derived from the Sayre equation using the same basis set as (a). (c) A potential map also derived under the same circumstances using Eq. (19). The data resolution for all these maps is 0.6 Å.

5.2. Method II: the Sayre equation and interpolative methods

As might be expected from the previous section, phase extension will work for this system with any of the interpolative methods, but not with the classic Sayre equation. As the starting point we used the same values as in the previous section. The use of the Sayre equation, and Eq. (19) from the same basis set as the previous section, resulted in the maps shown in Figs. 6(b) and 6(c), respectively. Virtually the entire structure is now clearly shown at close to atomic resolution; there are some small spurious peaks and some possible disorder (see Section 6). Least well resolved are the atoms in the third layer. Conventional Fourier methods can easily complete this structure. Extrapolation is much stronger than in the ab initio case, but the maps, however, are not as clean as their ME counterpart in Fig. 6a.

Carvalho et al. [32] have recently reported a ME reconstruction of the Si(111) 7×7 surface using both the electron diffraction data set used here and a smaller grazing-incidence X-ray one. In this case they used the atomic coordinates from the refined structure to give phase angles for all the non-bulk reflections which were then used as a basis set in a modified entropy maximisation. This is not a model-free reconstruction since the model is implicit in the phases; they are using ME methods to attempt to produce more detail in the potential maps, and thus examine deviations from the assumed model. This is different from the procedures used here where the basis sets are much smaller, the phases are not model derived, and thus the maps are truly model free.

Finally, Rius et al. have described an alternative direct methods approach based on a modified tangent formula derived from Patterson function arguments [33] which could be useful as a tool for solving surface structure; it needs to be tested with the Si(111) data.

6. Discussion

We have shown that one can, with due care, apply direct methods to solve surface structures.

The ab initio solutions encourage the view that this type of technique can be applied in general, although we need to define a standardised procedure, and this will require the study of many surface diffraction data sets. As is standard with direct methods, peaks in the potential maps may not have peaks exactly in the correct locations, and the relative heights may be wrong – however, as stressed earlier, there should be sufficient information to decode the rest of the structure by more conventional techniques. Phase extension shows that one can restore the potential rather well out to the available information limit of the measurements in a wholly routine manner.

It is worth commenting that we have deliberately looked at the worse possible case for the Si(111) 7×7 surface in the ab initio case, not using any other information than that available in the diffraction pattern. In many cases some information may be available from scanning tunneling microscopy (STM). For instance, since STM images of this surface clearly show adatoms, this information could have been incorporated into the original starting set – it would have fixed the phase of the (3,0) reflection and a few others. Even relatively low resolution electron microscope images could be used in the same fashion.

One complication which we have avoided here is the symmetry of the surface, which is generally an input parameter for the direct methods. While it is possible to scan over different possible symmetries, independent determination of these would be invaluable, although this is not always easy to determine from existing experimental techniques, although likelihood can in principle be used to resolve symmetry ambiguities: all possible symmetries are investigated, and the correct one (i.e. that which is most consistent with the measured intensity data) should have significantly higher likelihoods in the phasing tree than the remaining choices.

One interesting point is the disorder that is apparent in the restorations out to higher resolutions. The primary reason for this is that at larger angles, the kinematical approximation of a monolayer on a surface will break down. First, there is scattering from the long-range strain field associated with the reconstruction (by St.

Verdant's principle, to a depth approximately equal to the lateral dimensions of the reconstruction); as discussed previously [11,12] this contributes most significantly at larger angles. Second, there is dynamical diffraction of the surface reflections by the bulk lattice. While it is dangerous to generalize [33], this will tend to transport intensity from the strong, smaller-angle reflections out into the larger-angle ones. A secondary consequence of this is that it is difficult to obtain values for the Debye–Waller terms via a classical Wilson plot, as mentioned previously. It also turns out that crystal tilt can affect the Wilson statistics of the data, a point which will be discussed in more detail elsewhere [34].

Acknowledgements

C.J.G. acknowledges support from the EPSRC in the UK, from the Human Frontier Science Program and Eastman-Kodak, Rochester USA. L.D.M., D.G., C.C. and E.L. acknowledge support by the National Science Foundation on grant number DMR-9214505.

References

- [1] K. Takayanagi, Y. Tanishiro, M. Takahashi, S. Takahashi, J. Vac. Sci. Technol. A 3 (1985) 1502.
- [2] K. Takayanagi, Y. Tanishiro, M. Takahashi, S. Takahashi, Surf. Sci. 164 (1985) 367.
- [3] M.M. Woolfson, Acta Cryst. A43 (1987) 593.
- [4] C. Giacovazzo, Direct Methods in Crystallography, Plenum, New York, 1980.
- [5] M. Woolfson, Fan Hai-fu, Physical and Non-physical Methods of Solving Crystal Structures, Cambridge University, Cambridge, 1995.
- [6] L.D. Marks, R. Plass, D. Dorset, Surf. Rev. and Letters, to be published.
- [7] R. Plass, L.D. Marks, D. Dorset, submitted.
- [8] Y. Tanishiro, K. Takayanagi, Ultramicroscopy 27 (1989) 1.
- [9] R.D. Tweten, J.M. Gibson, Ultramicroscopy 53 (1994) 223.
- [10] P. Xu, L.D. Marks, Ultramicroscopy 45 (1992) 145.
- [11] L.D. Marks, P. Xu, D.N. Dunn, Surf. Sci. 294 (1993) 324.
- [12] G. Jayaram, R. Plass, L.D. Marks, Interface Sci. 2 (1995) 381.
- [13] E. Bengu, R. Plass, L.D. Marks, T. Ishimiya, P.M. Ajayan, S. Iijima, Phys. Rev. Lett. 77 (1996) 4226.
- [14] G. Bricogne, Acta Cryst. A 40 (1984) 410.
- [15] G. Bricogne, Acta Cryst. A 44 (1988) 517.
- [16] C.J. Gilmore, G. Bricogne, C. Bannister, Acta Cryst. A 46 (1990) 297.
- [17] G. Bricogne, C.J. Gilmore, Acta Cryst. A 46 (1990) 284.
- [18] G. Bricogne, in: B. Buck, V.A. Macaulay (Eds.), Maximum Entropy in Action, Oxford University, Oxford, 1991, p. 187.
- [19] K. Shankland, C.J. Gilmore, G. Bricogne, H. Hashizume, Acta Cryst. A 49 (1993) 493.
- [20] C.J. Gilmore, G. Bricogne, in: D. Moras, A.D. Podjarny, J.C. Thierry (Eds.), Crystallographic Computing 5: From Chemistry to Biology, Oxford University, Oxford, 1992, p. 298.
- [21] C.J. Gilmore, in: H.D. Flack, L. Parkanyi, K. Simon (Eds.), Crystallographic Computing 6: A Window on Modern Crystallography, Oxford University, Oxford, 1993, p. 25.
- [22] C.J. Gilmore, K. Shankland, G. Bricogne, Proc. Roy. Soc. Ser. A. 442 (1993) 97.
- [23] C.J. Gilmore, Acta Cryst. A 52 (1996) 561.
- [24] I.G. Voigt-Martin, D.H. Yan, A. Yakimansky, D. Schollmeyer, C.J. Gilmore, G. Bricogne, Acta Cryst. A51 (1995).
- [25] J. Karle, H. Hauptman, Acta Cryst. 9 (1956) 635.
- [26] R.H.T. Bates, M.J. McDonnell, Image Restoration and Reconstruction, Clarendon, Oxford, 1989.
- [27] C.J. Gilmore, J. Appl. Cryst. 17 (1984) 42.
- [28] C.J. Gilmore, S.R. Brown, J. Appl. Cryst. 22 (1988) 571.
- [29] R. Doll, M. Van Hove, (1995) submitted.
- [30] E. Landree, C. Collazo, R. Doll, M. Van Hove, L.D. Marks, in preparation.
- [31] R. Plass, L.D. Marks, Surf. Sci. 342 (1996) 233.
- [32] C.A.M. Carvalho, H. Hashizume, A.W. Stevenson, I.K. Robinson, Physica B 221 (1996) 469.
- [33] J. Rius, C. Miravittles, R. Allmann, Acta Cryst. A52 (1996) 634.
- [34] L.D. Marks, Ultramicroscopy 45 (1992) 145.